Solar Cell Materials by Design: Hybrid Pyroxene Corner-Sharing VO_4 Tetrahedral Chains

Article *in* ChemSusChem · February 2017

DOI: 10.1002/cssc.201700121

11 authors, including:

Fedwa El Mellouhi
Qatar Environment and Energy Research Inst…
68 PUBLICATIONS **645** CITATIONS
SEE PROFILE

Asma Marzouk
Qatar Environment and Energy Research Inst…
14 PUBLICATIONS **84** CITATIONS
SEE PROFILE

Stefano Sanvito
Trinity College Dublin
379 PUBLICATIONS **9,786** CITATIONS
SEE PROFILE

Fahhad Alharbi
Qatar Environment and Energy Research Inst…
90 PUBLICATIONS **465** CITATIONS
SEE PROFILE

ChemPubSoc Europe

DOI: 10.1002/cssc.201700121

CHEMSUSCHEM Full Papers

Solar Cell Materials by Design: Hybrid Pyroxene Corner-Sharing VO_4 Tetrahedral Chains

Fedwa El-Mellouhi,*[a] Akinlolu Akande,*[b] Carlo Motta,[c] Sergey N. Rashkeev,[a] Golibjon Berdiyorov,[a] Mohamed El-Amine Madjet,[a] Asma Marzouk,[a] El Tayeb Bentria,[a] Stefano Sanvito,[c] Sabre Kais,[a, d, e] and Fahhad H. Alharbi*[a, d]

Hybrid organic–inorganic frameworks provide numerous combinations of materials with a wide range of structural and electronic properties, which enable their use in various applications. In recent years, some of these hybrid materials—especially lead-based halide perovskites—have been successfully used for the development of highly efficient solar cells. The large variety of possible hybrid materials has inspired the search for other organic–inorganic frameworks that may exhibit enhanced performance over conventional lead halide perovskites. In this study, a new class of low-dimensional hybrid oxides for photovoltaic applications was developed by using electronic structure calculations in combination with analysis from existing materials databases, with a focus on vanadium oxide pyroxenes (tetrahedron-based frameworks), mainly due to their high stability and nontoxicity. Pyroxenes were screened with different cations [A] and detailed computational studies of their structural, electronic, optical and transport properties were performed. Low-dimensional hybrid vanadate pyroxenes $[A]VO_3$ (with molecular cations [A] and corner-sharing VO_4 tetrahedral chains) were found to satisfy all physical requirements needed to develop an efficient solar cell (a band gap of 1.0–1.7 eV, strong light absorption and good electron-transport properties).

Introduction

The recent past has witnessed a very persistent dedication to improve the performance of solar cells and to develop novel solar cell materials.[1–3] It is expected that the field of photovoltaics, especially as it relates to alternative and renewable energy, will grow further in the coming decades as the conventional fossil-fuel-based energy resources are depleted.[4,5] The most notable achievement arising from this effort is the emergence of a new generation of hybrid organic–inorganic perovskites as solar energy conversion materials.[6–8] Over just a few years, a variety of perovskite solar cells (PSCs) with different device designs have been developed with efficiencies already exceeding 20%.[9] Conceptually, the main requirements for the development of an efficient photovoltaic material are the following: i) the material should be a semiconductor with an electronic band gap in the 1.0–1.7 eV range (i.e., it must overlap with the intensity peak of the solar spectrum); ii) it must have strong light absorption; iii) the charge carrier transport must be good enough to allow the extraction of the photogenerated charge carriers.[10,11] Accordingly, a very large set of organic, inorganic, and hybrid semiconductors has been utilized to develop solar cells.[1,2] Until recently, the selection of the solar cell materials was mainly based on the available experimental data. Nowadays computational materials discovery has become a viable alternative way to find and design new materials before their experimental synthesis.[12–16] This direction is one of the main trends in the modern materials science and engineering and at present there is an enormous computational material discovery effort worldwide.[12,13] However, the field as a whole is still in its infancy and needs further standardization, database construction, intelligent database search, and experimental validation.[14]

Recent development in PSC research has allowed us to enlarge massively the materials screening space by considering hybrid organic–inorganic materials. These compounds were discovered in the late 1990s,[17] since when they have been developed for optoelectronic applications, mostly thanks to the work of Mitzi and co-workers.[18–23] Their potential use as light-absorbing media for solar cells was anticipated and suggested

[a] Dr. F. El-Mellouhi, Dr. S. N. Rashkeev, Dr. G. Berdiyorov, Dr. M. E. Madjet, Dr. A. Marzouk, Dr. E. T. Bentria, Prof. S. Kais, Prof. F. H. Alharbi
Qatar Environment and Energy Research Institute
Hamad Bin Khalifa University, Doha (Qatar)
E-mail: felmellouhi@hbku.edu.qa

[b] Dr. A. Akande
Department of Life Sciences, Institute of Technology
Ash Lane, Sligo (Ireland)
E-mail: akande.akinlolu@itsligo.ie

[c] Dr. C. Motta, Prof. S. Sanvito
School of Physics, AMBER and CRANN Institute
Trinity College, Dublin 2 (Ireland)

[d] Prof. S. Kais, Prof. F. H. Alharbi
College of Science and Engineering
Hamad Bin Khalifa University, Doha (Qatar)
E-mail: falharbi@hbku.edu.qa

[e] Prof. S. Kais
Department of Chemistry, Physics and Birck Nanotechnology Center
Purdue University, West Lafayette, Indiana 47907 (USA)

Supporting Information and the ORCID identification number(s) for the author(s) of this article can be found under http://dx.doi.org/10.1002/cssc.201700121.

a long time ago.[24] Fortunately, knowledge of hybrid materials accrued over the years is transferable and it has been used in PSCs, the synthesis of which is now focused around three-dimensional (3D) methylammonium lead iodide, $(CH_3NH_3)PbI_3$. During the developments of $(CH_3NH_3)PbI_3$, many organic and metallic cations have been employed. However, considering the enormous compositional space of such hybrid materials, the progress achieved to date could be just the tip of the iceberg and many more compounds remain to be discovered.

Another important lesson learned from the development of PSCs concerns the important role played by the channel transport.[25–27] Three-dimensional $(CH_3NH_3)PbI_3$ has a dipolar nature, which promotes the formation of different types of charged regions. These in turn serve as channels for charge-carrier transport. Similar channel transport is found for copper indium gallium selenide (CIGS) solar cells, where the grain boundaries form barriers for the holes, thus a very high concentration of electrons accumulates at the grain boundaries.[28] As a result, polycrystalline CIGS cells perform much better than their monocrystalline counterparts.

Herein we report the design of a new class of low-dimensional hybrid oxides based on inorganic oxide pyroxenes (tetrahedron-based frameworks).[29,30] The interest in these materials is mainly due to their high stability[31,32] and nontoxicity. Vanadate pyroxene oxide phosphors have been studied for more than three decades,[32] owing to their interesting photoluminescence and (photo)catalytic properties. In addition, vanadium is not toxic and widely abundant in the earth's crust. Vanadium can change its oxidation state from 5^+ to 2^+, enabling a variety of morphologies and structural network manipulations and offering a large spectrum of inorganic and hybrid stable structures that could be synthesized. In practice, materials with formula $[A]VO_3$, where $[A]=K^+$, Na^+, Cs^+, Rb^+, Ce^+, Bi^+, $NH4^+$, $(C2H5)NH3^+$ (EA), or $CH_3NH_3^+$ (MA) can all be accessed. Furthermore, inorganic and hybrid vanadium oxide powders are soluble and are used, for example, in the fabrication of supported vanadium oxide catalysts through liquid deposition followed by calcination on oxide supports such as SiO_2, Al_2O_3, TiO_2, or ZrO_2.[33] Various alternative synthesis routes have been reported for these materials, such as ink jet printing,[34] precipitation,[35]and atomic layer deposition (ALD).[36]

As we are interested in materials where the charge carrier can be confined, we focus herein on the low-dimensional vanadate pyroxene oxide phosphors, and in particular on the corner-sharing $[A]VO_3$ family, for example, $CsVO_3$. This compound is composed of chains of VO_4 tetrahedra supported by Cs cations. Despite its large band gap (E_g = 3.6 eV), $CsVO_3$ is well known for its good optical properties and slow electron–hole recombination, leading to a high quantum efficiency.[37,38] Our aim is to evaluate the optical and electronic transport properties of this class of materials. We will use computational design to identify materials with a band gap that is optimal for photovoltaic applications (1.0–1.7 eV)[10,11,39] by replacing Cs with a range of molecular cations. Certainly, the incorporation of molecules will generate additional stability[40–42] issues that will also be addressed. A detailed analysis can be found in the Supporting Information.

The paper is organized as follows: in the following section, we give a brief description of the computational methods used in this work and the procedures adopted for the material screening. In Results and Discussion, we first assess the electronic, transport and optical properties of experimentally known inorganic and hybrid pyroxene vanadates ($[A]VO_3$ with $[A]=Cs$, NH_4, or $(C_2H_5)NH_3$) to evaluate their potential as absorber in solar cells. Then, we present our newly designed hybrid pyroxene vanadates displaying a reduced electronic band gap, which is more suitable for absorbing the solar radiation in the visible range before concluding.

Computational Methods and System Screening

Computational methods

Electronic structure calculations were performed with density functional theory (DFT), as implemented in the Fritz Haber Institute ab initio molecular simulations (FHI-aims)[43] code. Structural optimizations were performed by using the generalized gradient approximation (GGA) of the exchange and correlation energy as parameterized by Perdew, Burke, and Ernzerhof (PBE). Long-range van der Waals (vdW) interactions were taken into account through the Tkatchenko–Scheffler (TS) scheme, which combines the GGA and a pairwise dispersive potential.[44] According to our tests, this scheme is more effective at reproducing the experimental volumes than GGA PBE alone. The TS functional is also crucial to describe the vdW forces governing the free energy landscape of such hybrid materials with respect to the molecular orientation.[40,45] The reciprocal space integration was performed over an $8\times8\times8$ Monkhorst–Pack grid.[46] A pre-constructed high-accuracy all-electron basis set of numerical atomic orbitals was employed, as provided by the FHI-AIMS "tight" default option. The Broyden–Fletcher–Goldfarb–Shanno algorithm[47] was used for the relaxation, with the crystal geometry determined by optimizing both the internal coordinates and the supercell lattice vectors with a tolerance of 10^{-3} eV Å^{-1} and without the constraint of orthogonal cell vectors.

A key additional part of our theoretical analysis was enabled by refined calculations of the optical and electronic properties of the most promising compounds. In this case, we used higher—more computationally expensive—levels of theory, such as non-collinear calculations taking into account spin–orbit coupling and the use of the HSE06 hybrid functional, as well as the G0W0 method.[48] Hence, additional DFT calculations were performed with the projected augmented wave (PAW) method implemented in the Vienna ab initio simulation package (VASP).[49] In this case, the basis set was plane wave and we used an energy cutoff of 520 eV.

Finally, charge transport was estimated by means of the semiclassical Boltzmann theory within the constant relaxation time approximation, as implemented in BoltzTrap code.[50] A dense mesh of 30000 *k*-points over the full Brillouin zone was employed in this case.

System screening

Herein we have considered materials having a $A^{+1}B^{+5}Y_3^{-2}$ structure, that is, materials composed of 1^+ and 5^+ cations alongside three 2^- anions. Vanadate compounds belong to this family. Previously reported syntheses of vanadates have incorporated a wide range of inorganic and molecular cations, with their structural data being made available in the ICSD database.[52] Inorganic vanadate compounds MVO_3 ($M^+ = Li^+$, Na^+, K^+, Tl^+, Rb^+, Cs^+) exhibit interesting optical properties.[37,53] However, structures incorporating molecular cations, such as NH_4^+ or $(C_2H_5)NH_3^+$ (EA), are not very well known. The optical and electronic transport properties of the hybrid pyroxene vanadates (see the section on the assessment of existing inorganic and hybrid pyroxene vanadates) demonstrate their suitability for solar cell applications. Nevertheless, these potential for applications have not been tested to date because of their large band gap. Hence, our design strategy targeted previously unreported hybrid pyroxene structures with molecular cations that conserve the 1D zigzag chain structure of the VO_4 tetrahedra while displaying smaller optical band gaps to enable efficient visible-light absorption.

The screening was performed over different steps in which the pool of candidate materials was reduced at each step. The criterion for the selection of the surviving candidates at each step is called the descriptor. This is a simple quantity that can be calculated from the electronic band structure. One such descriptor is the band gap. The overall workflow for the screening process adopted in the present study is outlined in Figure 1. Our systematic approach begins by identifying stable crystal structures based on their chemical composition. The family of systems explored in this study comprises of $[A]VO_3$, where the cations A^+ investigated are NH_4^+, PH_4^+, H_3O^+, H_3S^+, $CH_3NH_3^+$, $CH(NH_2)_2^+$, and $CH_3CH_2NH_3^+$. Their molecular structures are shown in Figure 2, together with the calculated dipole moments.

Although there is obviously a larger number of possible cations than one can study, only cations with a size comparable to that of Cs^+ are expected to have structural stabilities similar to the existing $CsVO_3$, and thus deserve our attention.

Starting from the inorganic $CsVO_3$, the structure of which is composed of chains of VO_4 tetrahedra supported by Cs cations, we replace Cs with the positively charged molecules shown in Figure 2. The resulting prototypes are fully relaxed by using the standard GGA-PBE functional. The GGA gives reliable structural properties for such complex systems, especially when the vdW interactions are taken into account, as in this work.

Our first elemental descriptor is the GGA-PBE band gap, E_g^{PBE}, which is easily accessible and physically intuitive. Although the GGA functional is known to yield good structural accuracy, it usually underestimates the band gap of semiconductors and insulators. Therefore, calculations using exchange-correlation functionals beyond GGA are required to obtain

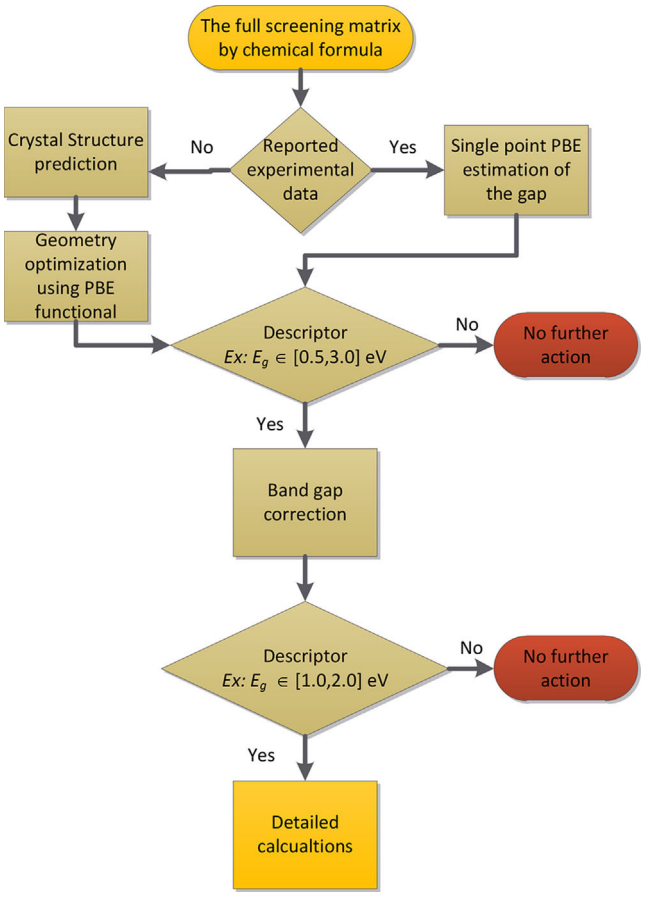

Figure 1. Workflow of the screening process implemented in this work. Stable crystal structures are either extracted from experimental databases or predicted empirically based on their chemical composition.[51] These structures are used as an initial estimate for the generation of new geometries, which are in turn fully optimized by using DFT. The suitability of a given material for solar cell applications is assessed based on the band gap descriptor, that is, by verifying that the PBE band gap falls in the interval 0.5–3.0 eV. New calculations at the HSE06 level are performed only for those structures that are deemed suitable at the first stage. At this point, a second screening process takes place, where materials are selected only if their HSE06 band gap is in the narrowed interval of 1.0–2.2 eV. For these compounds, additional calculations (e.g., transport properties) are performed.

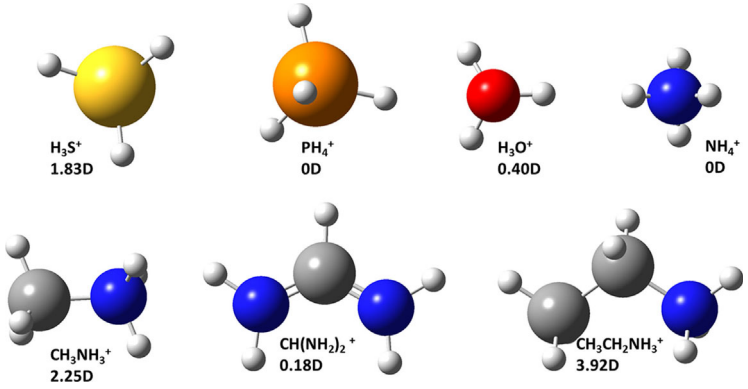

Figure 2. Positively charged cations and their corresponding calculated dipole moments (in Debye). Starting from the $CsVO_3$ supercell, each Cs is substituted by one of the positively charged molecules. Color code: C = grey, H = white, O = red, N = blue, P = orange, S = yellow.

a better estimate of the actual gap, E_g. However, as an initial crude step, the GGA-PBE band gaps are still taken as first descriptor. In particular, we advance to the next step those materials for which $E_g^{PBE} = 0.5–3$ eV. However, we also take into account that spin–orbit coupling would in some cases result in significant splitting of energy levels and hence lead to a lowering of the band gap by as much as 1 eV, as in the case of Pb-based perovskite materials. Hence, a 3 eV upper limit for the band gap constitutes, in our opinion, a safe general threshold over a wide range of materials, not limited to the vanadates screened here, and would ensure that no potentially interesting candidates be missed.

Next, the calculation of the optical properties is refined by using a higher-level, more accurate functional. We consider the inclusion of exact exchange for the most promising compounds. Calculations are made with the hybrid functional HSE06[53] (to give E_g^{HSE06}) and include spin–orbit coupling (SOC) and are applied to the structures obtained from the previous round of screening. The acceptable range of E_g^{HSE06} at this point is narrowed down to 1.0–2.2 eV. Materials progressing through this second stage are further investigated and their transport properties are calculated.

Results and Discussion

In this section, we present results concerning the structural properties, the band structure, the projected density of states (PDOS), the polarization, the optical spectrum, and the carrier transport. We analyze both existing materials and those selected by our screening protocol.

Assessment of existing inorganic and hybrid pyroxene vanadates for photovoltaic applications

Our starting system is the inorganic $CsVO_3$, for which both theoretical and experimental data are available. This material belongs to a family of vanadium oxide phosphors, and it holds potential as a lighting medium due to its excellent photoluminescence characteristics with almost perfect quantum efficiency[37,53] It has an orthorhombic pyroxene lattice with the VO_4 tetrahedra joined at two corner oxygen atoms to form a one-dimensional chain structure (see Figure 3) with an $O-\widehat{O}-O$ angle of 180° and an O rotation of 0°.[32] The VO_4 sheets and the Cs cation layers are then alternately stacked along the *a* axis.[37]

The distortion of the VO_4 tetrahedra characterized by the two single V–O and two double V=O bonds and six $O-\widehat{V}-O$ bond angles is well known for this compound and was attributed to the large cation size (Cs in this case)[37] The degree of distortion of the VO_4 tetrahedra is expressed by two parameters: the distance Δd_n and the angle Δa_n averaged over all V–O distances and $O-\widehat{V}-O$ angles measured for the tetrahedral units in the system (see definition in Ref. [55]), as given by Equations (1) and (2).

$$\Delta d_n = \sum \left| (V-O)_d - \overline{(V-O)_d} \right| / 4 \qquad (1)$$

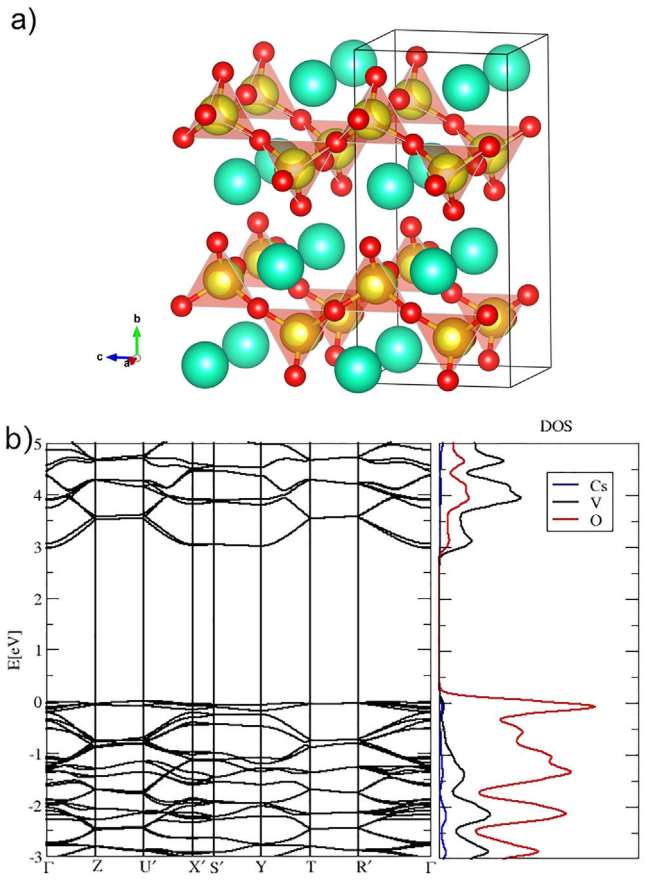

Figure 3. $CsVO_3$ structural and electronic properties: a) Experimental unit cell taken from Ref. [32] (ICSD database code: 1489). b) Corresponding band structure and PDOS. Color code: Cs = green, Vanadium = yellow, oxygen = red.

$$\Delta a_n = \sum \left| \left(O-\widehat{V}-O\right)_a - \overline{(O-\widehat{V}-O)_a} \right| / 6 \qquad (2)$$

Correlating and relatively large values of Δd_n and Δa_n were identified in several previous reports.[37,53] This feature is believed to account for the superior optical properties of $CsVO_3$, since the resulting crystal field impacts the band structure by lifting the band degeneracy (see Figure 3 b). In addition, it was postulated that exciton diffusion and lifetime along the VO_4 chain structure are strongly enhanced due to the cation's induced polarization and the elongation in the interchain distance. In the hybrid vanadates, these two properties correlate with the molecule's dipole moment and the ionic size, respectively,[37] as discussed below.

Two hybrid vanadate systems, namely ammonium vanadate (NH_4VO_3) and ethylammonium vanadate [$(C_2H_5)NH_3VO_3$ or $EAVO_3$], have been previously reported, the data for which are available in the ICSD database.[32,52,56] Their crystal structures have been fully relaxed and then their band structures calculated. By decreasing the ionic radius of Cs^+ to that of NH_4^+, the interchain distance along the *x* (d_x) and *y* (d_y) directions decreases from $d_x = 5.37$ Å and $d_y = 6$ Å for $CsVO_3$ to $d_x = 4.8$ Å and $d_y = 5.12$ Å for NH_4VO_3 (Figure 4). This indicates a more closely packed tetrahedral chain structure in the case of NH_4VO_3.

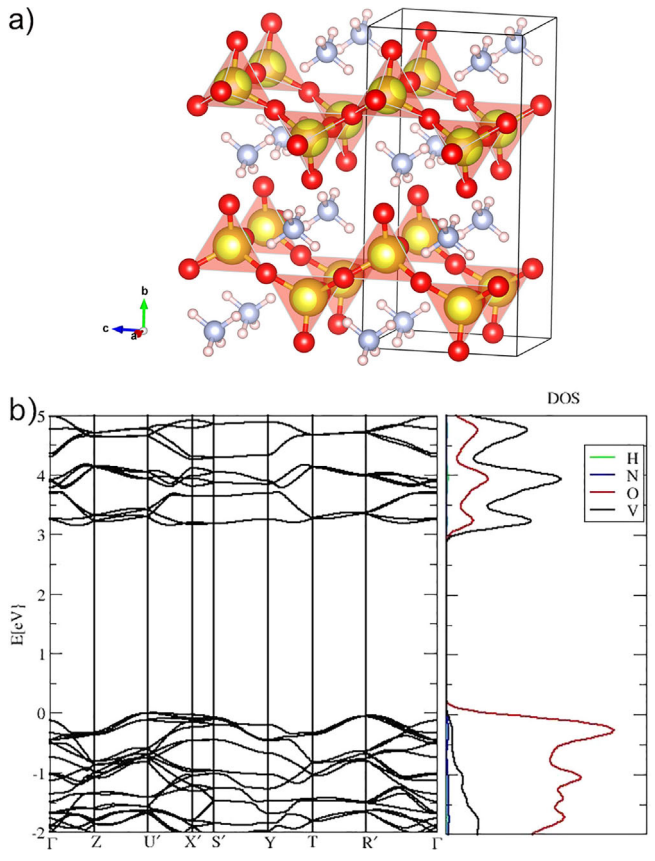

Figure 4. Ammonium-vanadate structural and electronic properties. a) Experimental unit cell taken from Ref. [32] (ICSD database code: 1487). b) Corresponding band structure and PDOS. Color code: V = yellow, O = red, N = light blue, H = light pink.

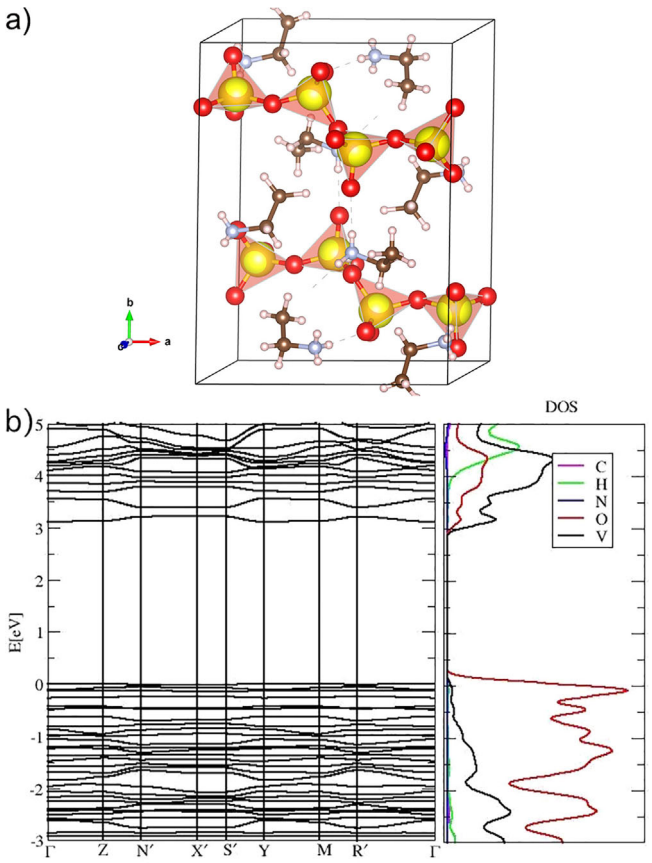

Figure 5. Ethylammonium vanadate structural and electronic properties. a) Experimental unit cell taken from Ref. [56] (ICSD database code: 110483). b) Corresponding band structure and PDOS. Color code: V = yellow, O = red, N = light blue, C = brown, H = light pink.

When the NH_4^+ ions are introduced, the crystal shows a deformed VO_4 octahedron with a broken T_d symmetry, as found in some inorganic counterparts such as $CsVO_3$ and KVO_3. The symmetry lowering results in a split in the degeneracy of the V^{5+} d orbitals, allowing spin-forbidden transitions, possibly leading to enhanced luminescence[37,53] On increasing the ionic radius by exchanging Cs for EA, the interchain distance is increased to $d_x = d_y = 7.5$ Å. At the same time, the one-dimensional chains undergo considerable distortion, bending and twisting (the angle is denoted by Φ). The symmetry lowering that occurs when going from an orthorhombic to a triclinic symmetry can be appreciated in Figure 5 and quantified in Table 1.

In the case of NH_4VO_3, the standard deviation of the four V–O bond lengths and six $O-\widehat{V}-O$ bond angles are 4.8–5 %

Table 1. Number of atoms per unit cell N_{atoms}, lattice parameters (a, b and c) and lattice vector angles (α, β, and γ), distances between the two VO_4 extended chains along the x (d_x) and y (d_y) directions as well as the twisting angle of the tetrahedra with respect to the V–V axis (Φ) for the screened pyroxene vanadates with general formula [A]VO_3.

[A]	N_{atoms}	a [Å]	b [Å]	c [Å]	α [°]	β [°]	γ [°]	d_x [Å]	d_y [Å]	Φ [°]
Cs[a]	20	5.39	12.25	5.78	90	90	90	5.4	6.1	0
Cs[b]	20	5.46	12.42	5.86	90	90	90	–	–	–
NH_4[c]	36	4.88	11.99	5.91	90	90	90	4.9	6.0	0
PH_4	36	5.63	12.36	5.88	89.52	89.73	90	5.6	6.3	3.5, 2
H_3O	32	5.28	11.23	5.72	89.1	92.2	90.0	5.3	5.5	6, 4
H_3S	32	5.25	13.60	5.88	91.2	90.5	91.45	5.2	6.8	2.5, 1.2
CH_3NH_3	48	5.84	13.24	5.91	89.46	88.7	94.2	5.8	6.6	2.5, 8
$CH(NH_2)_2$	48	6.2	13.65	5.97	89.1	90.7	106.4	6.2	6.7	2.7, 3.7
$CH_3CH_2NH_3$[d]	120	10.82	14.33	7.47	100.8	91.4	90	7.5	7.5	16

[a] Experimental structure taken from Ref. [32]. [b] This work, fully relaxed with PBE + vdW. [c] Experimental structure taken from Ref. [32]. [d] Experimental structure taken from Ref. [56].

and 0.2–0.9%, respectively. These deviations are due to corner sharing between the VO_4 tetrahedra forming a chain. To keep the chain coordination, the VO_4 tetrahedra need to distort under the influence of the dipole moment, as well as the size and the strength of the hydrogen bonding induced by the molecular cation. Interestingly, low-temperature powder diffraction and DFT calculations[57] show that ammonium NH_4^+ displays one moderate bifurcated hydrogen bond and two trifurcated N–H–O hydrogen bonds. This leads to the formation of two strong hydrogen bonds.

Turning now our attention to the electronic properties, the band structure and the PDOS of $CsVO_3$ are shown in Figure 3. The system has an indirect band gap of approximately 3 eV. Interestingly the indirect gap originating from the location of the valence-band maximum (VBM) at (0.5, 0.0, 0.35)$2\pi/a$ and conduction-band minimum (CBM) at (0.5, 0.0, 0.0)$2\pi/a$ is close to a direct one (within a few meV) located at the X′ [(0.5, 0.0, 0.0)$2\pi/a$] high-symmetry *k* point. This is in virtue of a rather flat band placed at the very top of the valence band. Such behavior has been reported for other perovskite structures, such as $BiVO_3$[58] and for lead halide perovskites,[45,59] and it is believed to account for the slow electron–hole relaxation[60] and recombination.[61,62] The VBM is dominated by O 2p orbitals with minor contributions from V 3d orbitals, whereas the CBM is a hybrid band between the O 2p and the V 3d states, dominance by the V 3d orbitals.

The calculated electronic structure around the gap energy region must be entirely attributed to the electronic states of the VO_4 tetrahedra. Although the O 2p orbitals make the dominant contribution to the valence band, its lower energy region contains a significant V 3d contribution. These electronic states originate from the bonding e_g and t_{2g} orbitals in the VO_4 structure. Upon moving toward the top of the valence band, the V 3d contribution decreases as the bonding states give way to the O 2p nonbonding ones. The states at the top of the valence band originate from the t_1 orbitals of VO_4. In contrast, the conduction bands receives contributions from the t_{2g}, the e_g and the a_1 antibonding orbitals with V 3d and O 2p orbital character. Cs states appear to contribute far from the band edges.

We have also performed both HSE06 and G0W0 calculations on top of PBE[63,64] and found the band gap opening to 4.5 eV with no notable effect due to spin–orbit coupling. The reported experimental band gap is 3.6 eV, which is in the near-UV A range. HSE06 appears to overestimate the band gap for vanadates, a feature typical for this class of materials as in the case of $BiVO_3$.[58] Nevertheless, we use the original formulation of HSE06, keeping in mind that the resulting band gaps for the newly designed materials might be overestimated by as much as 1 eV.

Similarly, the electronic structure calculations for ammonium vanadate reveal that the band gap remains around 3 eV (Figure 4b), which is comparable to that of its inorganic Cs-based counterpart. In addition, an analysis of the band structure and the PDOS demonstrates that the molecule-derived energy levels have spectral amplitude only at energies deep into the conduction and valence bands. The valence states have a dispersion larger than that found for $CsVO_3$ which we attribute to the shorter distances between the VO_4 tetrahedra, and hence, to a stronger O–O interaction. The conduction bands, however, display a slightly stronger degeneracy lifting. These differences in the electronic structure due to structural parameters (governed by the connectivity of the VO_4 octahedral network) are well known as crystal field effects. These impact directly the light absorption, as well as the electron- and hole-transport properties (see below).

For ethylammonium vanadate, the reported experimental structure has triclinic symmetry with a large 120-atom unit cell containing eight tetrahedral VO_4 units. The tetrahedra are connected by sharing corners and they are twisted with respect to each other, leading to bent chains (see Figure 5 and Table 1). This structural feature might be induced by both the size and the dipole moment of the EA molecule, causing the VO_4 tetrahedra to twist. This reduces the degree of overlap between the V and O orbitals and hence suppresses hybridization. The band structure for $EAVO_4$ (lower panel of Figure 5) displays two flat atomic-like bands that span across the entire Brillouin zone path. The state at the VBM is a pure oxygen p state, whereas the CBM is located at 3 eV, leading to a band gap of 3 eV. The fact that the cell is severely non-orthorhombic might also account for this band degeneracy lifting. This route might then be used to reduce the band gap in the hybrid pyroxene vanadates. However, the charge-transport properties might be negatively impacted along the chains due to the weak overlap between V and O within the tetrahedral chains.

In summary, similar to $CsVO_3$, the hybrid vanadates' band structures feature a lifted degeneracy of the bands, which allows spin-forbidden transitions to take place, possibly leading to enhanced photoluminescence.

Optical properties

The optical absorption properties of the inorganic pyroxene vanadate oxides $[A]VO_3$ (A = K, Rb, Cs) were experimentally measured by Nakajima and co-workers,[37,53] who confirmed that the origin of their intense luminescence is due to the charge transfer transition within the VO_4 tetrahedra. $CsVO_3$ gave the best photoluminescence properties and an internal quantum efficiency of 87%.[37]

The calculated imaginary part of the frequency-dependent dielectric function calculated from PBE is shown in Figure 6a for $CsVO_3$ and for the hybrid NH_4VO_3. The light absorption spectrum is anisotropic and the first dominant peak is along the *z* direction, corresponding to the direction of the VO_4 chains. This anisotropy is mainly due to the 1D chains network. Thus, the crystal is optically biaxial, a fact that can be used for many optical applications.[65–68] The action of the crystal field in lifting the degeneracy of the electronic bands due to the VO_4 tetrahedral deformation impacts similarly the light absorbing properties through the appearance of multiple peaks. The absorption features of NH_4VO_3 are, both qualitatively and quantitatively, similar to those of its inorganic counterpart $CsVO_3$. This suggests that hybrid vanadates might exhibit high quantum efficiencies and possibly good photovoltaic properties

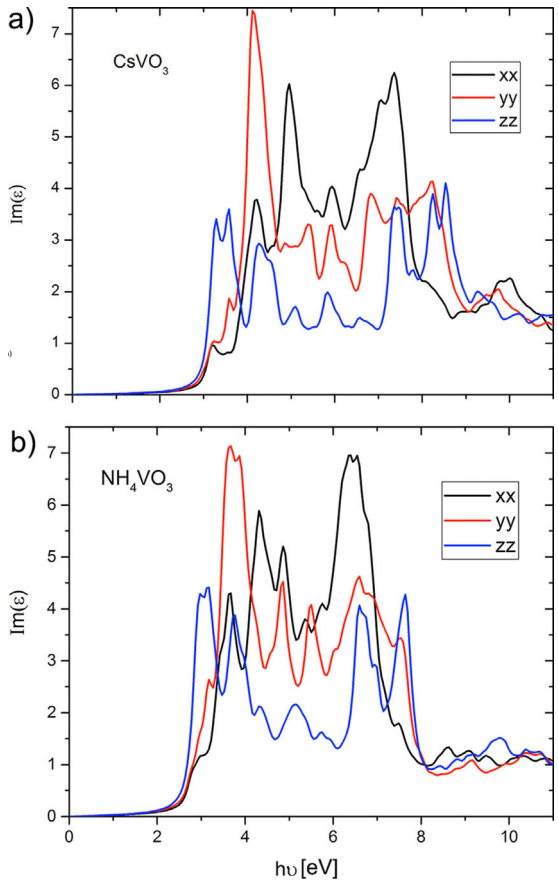

Figure 6. Imaginary part of the frequency-dependent dielectric functions of $CsVO_3$ (a) and NH_4VO_3 (b). Note the absorption anisotropy resulting from the strong crystal field present in both cases as a consequence of the VO_4 tetrahedral deformation.

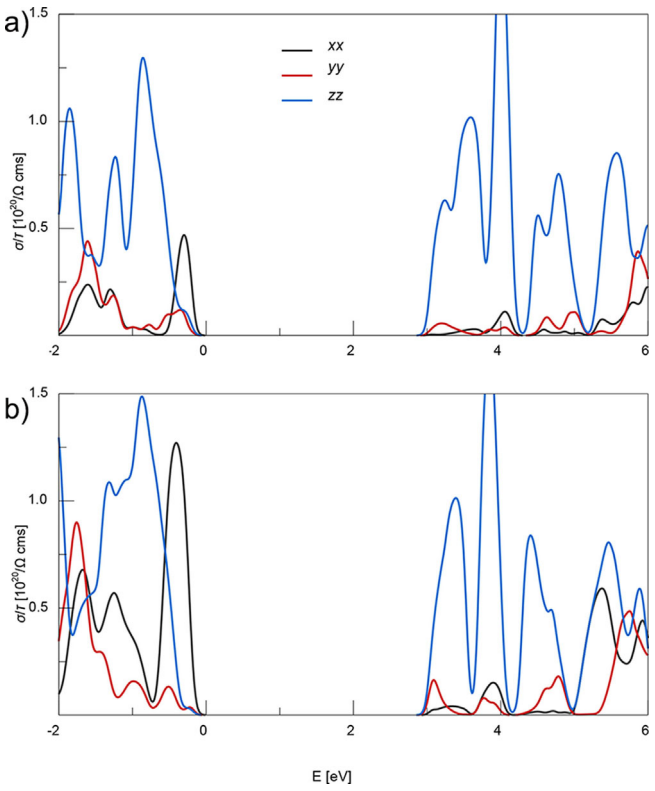

Figure 7. Static electrical conductivity σ/τ as a function of the chemical potential for $CsVO_3$ (a) and NH_4VO_3 (b). The black, red, and blue lines represent the conductivity tensors σ_{xx}, σ_{yy}, and σ_{zz}, respectively.

once their band gap is customized to be in the visible region. With these positive results in hand, we next looked at the charge-transport properties of the organic and inorganic pyroxene vanadates.

Transport properties

Figure 7 shows the electrical conductivity along various directions calculated by using the Boltzmann semiclassical theory described above. Bearing in mind that we are using here a single relaxation time approximation, it is clearly shown that the charge transport is significantly easier along the *z* direction (σ_{zz} conductivity tensor). This is along the axis of the 1D tetrahedral VO_4 chains and this property is shared by the hybrid material and the inorganic $CsVO_3$. Along with the prominent σ_{zz} contribution, we also observe a large peak in the σ_{xx} tensor close to the valence edge, which indicates hole conductance perpendicular to the chains. Interestingly, for NH_4VO_3, this peak is more than twice the size of that for $CsVO_3$. A possible explanation for this difference can be found in the fact that the organic compound, NH_4VO_3, is more closely packed than its inorganic counterpart $CsVO_3$. The NH_4VO_3 unit cell volume is approximately 12% smaller than that of $CsVO_3$ (see the distances d_x and d_y, Table 1). This tighter structure results in a more dispersive valence band maximum in NH_4VO_3 (see Figure 4). As a consequence the average group velocity is larger and so the conductivity. Similar considerations can be made to explain the origin of the small σ_{yy} contribution at the conduction edge. Indeed, a volume contraction occurs in the x–y plane, explaining why σ_{zz} has the same magnitude for the two compounds.

From the $CsVO_3$ in terms of Van der Waals radii (for schematics, see the Supporting Information, Figure S1 a), one can clearly observe strong overlap of the chains along the *z* direction. In contrast, the *y* direction consists of an alternating O–Cs–O network, which contributes to the conductivity (and the DOS) very far from the band edges. This explains why both the electron and hole σ_{yy} conductivity tensor is small around the band edges. As far as the σ_{yy} conductivity tensor is concerned, we observe that the chain remains disconnected along the *y* direction regardless of whether the atomic or the van der Waals radii are considered. Although the connectivity along the *z* direction is similar for $CsVO_3$ and NH_4VO_3, that across the direction of the VO_4 chains is more pronounced for NH_4VO_3, which then presents a larger conductivity in the plane perpendicular to the chains.

In closing this section, we note that overall the existing hybrid vanadate pyroxenes seem to feature optical and transport properties that are comparable to those of the well-studied inorganic counterpart $CsVO_3$.[69] This means that potentially the only aspect limiting NH_4VO_3 as a medium for solar cell applications is its large band gap. Recently, our group has shown

that it is possible to tune the band gap of hybrid materials by using appropriate molecular cations that enhance the electronic coupling through hydrogen-bond manipulation.[40–42] In the next section, we will follow this strategy and focus our screening effort on: i) reducing the band gap in this class of materials, ii) allowing a better absorption in the visible range, iii) keeping the 1D VO_4 chain structure, and iv) distorting the tetrahedra. This last feature might ensure an efficient charge separation and an enhanced exciton diffusion and lifetime, thus improving collection of the photogenerated charges.

Materials screening

In hybrid materials, computing accurate structural parameters is crucial to understand the way in which the size, the structure, and the interaction between the organic and inorganic sublattices affect each other and the materials' properties. This is particularly important when one designs new compounds, so that in all cases we perform full relaxation. Binek et al. proposed that the dipole moment of the molecular cations stabilizes hybrid perovskites and leads to long carrier lifetimes.[70] In fact, the appropriate balance between the number of hydrogen bonds formed between the cation and the inorganic cage against the strength of these bonds was deemed as the principle stabilizing factor. Moreover, cation substitution with the various positively charged molecules, displaying a variety of dipole moments and thus generating different interaction strengths,[71] was reported as an effective tool for band gap manipulation.

Our initial test calculations demonstrated that geometry optimization of sufficiently large supercells is crucial to obtain reasonably converged initial structures. For example, the $CsVO_3$ perovskite primitive unit cell, containing 5 atoms, is unstable under geometry optimization and relaxes to the pyroxene structure. In doing so, the band gap opens to 3 eV (Figure S2). This is a clear indication that substitution of Cs with molecular cations with different symmetries and dipole moments might require careful attention.

The lattice and unit cell structural parameters of all the compounds investigated, either existing or our constructed prototypes, are shown in Table 1. Most of the compounds adopt a low-symmetry triclinic lattice with *P*1 space group, but at the same time maintain the E-chain ordering of the VO_4 tetrahedra.[32] Fully relaxed structures containing different molecular A sites induce sizeable structural changes, which affect the volume. The geometry of the cell and the internal bending and patterning of the VO_4 tetrahedral network as well as the V–O–V bond angle reflect the degree of the hybridization between the V and O orbitals.[55] Table 2 gives the corresponding PBE gaps, E_g^{PBE}, and the difference between the PBE gap of a given material and that of the existing NH_4VO_3 pyroxene vanadate, ΔE_g. According to our procedure, accurate band gaps are calculated only for the candidates that show a significant band gap reduction due to the cation substitution (i.e., H_3S^+).

Details of the VO_4 tetrahedra deformation metrics, displaying the average V–O bond length, the V–O–V bond angle, and the average twisting angle around the V–V axis, are given in Table 3 for the experimentally reported inorganic and hybrid pyroxene vanadates together with the designed compounds reported herein with lower electronic band gaps. The degree of VO_4 tetrahedra deformation (Δd_n and Δa_n, Table 3) is similar for all materials analyzed except for H_3SVO_3, which has a larger Δa_n value than the other compounds. The tetrahedral deformation originates from the moderate hydrogen-bond formation between H_3S^+ and the VO_4 tetrahedron (see the Supporting Information), thus inducing the crystal field electronic band splitting, as well as the anisotropies observed in optical and transport properties.

With H_3O^+ and PH_4^+, the chain-like characteristics of the crystal structure were not altered except for a bending and twist of the VO_4 tetrahedral chain, reaching up to 6°. Interestingly, PH_4^+ has no dipole moment, due to the balanced charge distribution on its H atoms. Thus, it is not affected by the strong electronegativity of the oxygen ions and forms bifurcated and weak P–H–O hydrogen bonds. In contrast, H_3O^+, although smaller in size, has a small dipole moment of 0.4 Debye, which leads to a moderate but balanced O–H–O hydrogen bond with the V=O bonds.

The band gaps of H_3OVO_3 and PH_4VO_3 are indirect, measuring 2.81 eV and 2.86 eV, respectively. As such, their gap reduced by about 0.2 eV in comparison to that of NH_4VO_3. This is attributed to the crystal field, which lifts the degeneracy of the VBM and CBM, similarly to the more pronounced effect observed for $EAVO_3$. The PDOS shows that the CBM and VBM remain dominated by the V and O states, whereas the molecu-

Table 2. Band gaps resulting from the first screening step using standard DFT PBE calculations as a first descriptor of designed hybrid [A]VO_3 vanadates and the resulting band gap reduction (ΔE_g) due to the cation substitution. NH_4VO_3 system is used as a reference for the band gap reduction. Bold face data indicate candidates that show a significant band gap reduction due to the cation substitution that avail to more accurate HSE06 and G0W0 calculation.

[A]	Eg^{PBE} [eV]	ΔE_g [eV]
NH_4	3.0	–
PH_4	2.86	−0.14
H_3O	2.81	−0.19
H_3S	1.68	**−1.32**
CH_3NH_3	2.62	−0.38
$CH(NH_2)_2$	2.99	0
$CH_3CH_2NH_3$	2.99	0

Table 3. VO_4 tetrahedral deformation properties for various cations, displaying the average V–O bond length $d_{(V-O)}$ and the V–O–V bond angle ($O-\widehat{V}-O$). The degree of VO_4 tetrahedral deformation, quantified by Δd_n and Δa_n, is similar for all the materials analyzed except for H_3S, which has a larger V–V twisting angle (Δa_n) than the remaining compounds.

Molecule	$d_{(V-O)}$ [Å]	Δd_n [10^{-2} Å]	$O-\widehat{V}-O$ [°]	Δa_n [°]
Cs	1.72	6.73	147	1.0
NH_4	1.73	7	145	1.5
CH_3NH_3	1.73	6.53	151, 138	0.33
H_3S	1.73	5.14	144, 141	2.11

lar states start to contribute weakly from 1 eV below the VBM and 2.5 eV above the CBM.

Interestingly, in the case of H_3S^+, a pronounced peak appears above the O 2p valence bands, resulting in the reduction of the electronic band gap from 3.0 to 1.7 eV (Figure 8). The first intermediate state and band originates from the S 3p orbitals, whereas the subsequent four bands are hybrids of S 3p and O 2p orbitals. This is the first occurrence of the emergence of molecular states in the gap-forming intermediate bands; that is, it is the first time that we find an electronic contribution of the molecule to the band gap states. From a structural point of view, the average V–O bond lengths are 1.73 Å and the V–O–V angles are 144° and 142° for each chain, whereas the twisting angle does not exceed 2.5°. This suggests that the sizeable band-gap reduction might be caused by a mechanism different from the crystal field effect.

A close examination of the structure reveals that H_3S^+ donates one hydrogen that becomes bonded to the nontetrahedrally connected oxygen (V=O), hence deprotonating the molecule to form H_2S. The S–H–O distance is 3 Å, which is smaller than the sum of vdW radii of the complex (O: 1.52 Å; H: 1.2 Å; S: 1.8 Å). The nonbifurcated or linear S–H–O bond angle is 170°, indicating strong hydrogen-bond formation (a detailed analysis of the strength of the hydrogen bond can be found in Figures S4–S6 and Table S1). This hydrogen bond analysis confirms that S–H–O fulfils all the criteria of the recent definition of the hydrogen bond by the IUPAC.[72] The large dipole moment of the molecule, associated with the strong electronegativity difference between S and O, is the primary driver for the molecular deprotonation and the formation of this strong hydrogen bond.

We calculated a band gap of 2.7 eV by using HSE06, whereas the spin–orbit coupling seems to be quantitatively irrelevant for this class of materials. As mentioned earlier in the case of $CsVO_3$, HSE06 with 25% exact exchange most likely overestimates the band gap in this case as well. Therefore, higher and more accurate levels of theory might be needed to predict the correct band gap for this compound. Nevertheless, its band gap remains within the range of visible light. Recently, lead-free hybrid perovskites with optical band gaps larger than 2 eV have been synthesized and explored for photovoltaic applications.[73,74] This is an interesting direction for H_3SVO_3 too.

Continuing our analysis, we observe that MA^+ induces a band gap reduction of 0.38 eV. Its crystal, band structure and PDOS are shown in the lower part of Figure 8. Interestingly, no molecular states appear near the band edges. However, sizeable band splittings can be observed on both the VBM and the CBM. Despite the large dipole moment of MA, the electronegativity difference between N and O seems insufficient to trigger the deprotonation of the amine group. The N–H–O distance is 2.8 Å, which is smaller than the sum of the vdW radii of the complex (O: 1.52 Å, H: 1.2 Å, N: 1.55 Å). The nonbifurcated N–H–O bond angle is 161°, indicating a hydrogen bond of moderate strength. Hence, one may conclude that the band gap reduction is dominated by the crystal field splitting, as in the case of $EAVO_3$, which is probably due to the large twist

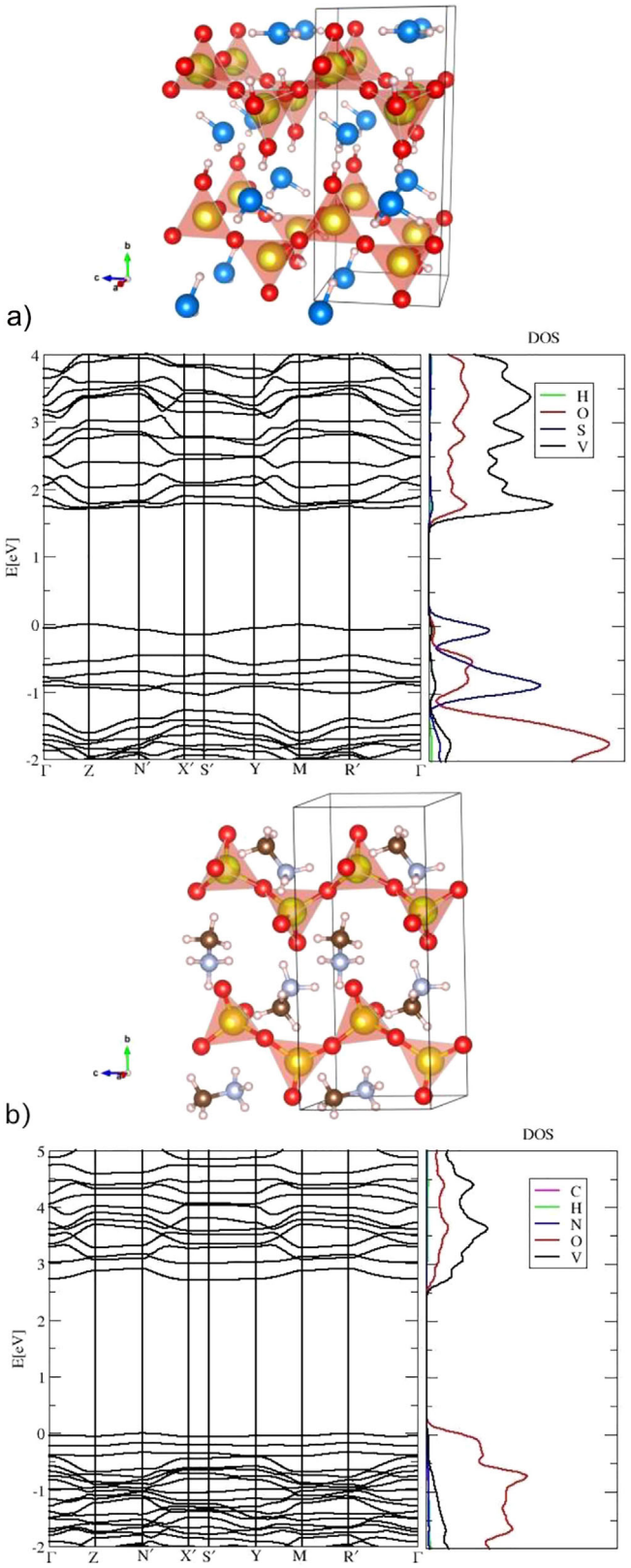

Figure 8. Crystal structures, electronic band structures, and PDOS showing the impact of substituted cations [A] = H_3S^+ (a) and $CH_3NH_3^+$ (b) on reducing the electronic band gap of hybrid pyroxene vanadates [A]VO_3.

angle reaching 8° in one of the chains and the increase in the interchain distance.

Interestingly, larger cations, such as $CH(NH_2)_2^+$ (FA^+), which is nowadays widely used in PSCs,[9,59,75,76] do not seem to alter the electronic properties or to induce the desired band gap reduction despite its large ionic radius (Figure S3 a). The N states and bands hybridized with O 2p states appear at the top of the valence band and the splitting of the CBM is of a magnitude comparable to that in the H_3S^+ case. Neither mechanism identified in this work, that is, crystal field or hydrogen bond formation, seem to be efficient to reduce the band gap in this case. This fact suggests that the molecule's weak dipole moment plays an important role as well. It is worth noting that the two amine groups in the FA^+ molecule ensure good connectivity between the chains along the *x* and *y* directions, which might account for the nitrogen states observed near the VBM.

Chemical stability calculations against phase separation revealed that the newly designed materials H_3SVO_3 and $CH_3NH_3VO_3$ are stable (Table S2). In the case of H_3SVO_3, the stability enhancement is attributed to the hydrogen-bonding effect (Figures S4–S6). These findings are in line with our previous reports.[40–42]

Finally, the associated absorption spectra for the screened materials are calculated in the independent particle approximation and plotted in Figure 9. Most of the hybrid vanadate-screened phosphors show comparable optical properties to the inorganic $CsVO_3$, which is known for its good photoluminescence and high quantum efficiency. Compounds with reduced band gap due to hydrogen bond formation and molecular deprotonation, such as H_3S^+, are expected to have superior light absorption properties due to the appearance of absorption peaks around the visible light frequency.

Conclusions

We have reported a detailed computational study of the structural, electronic, optical and transport properties of low-dimensional hybrid pyroxene corner-sharing VO_4 tetrahedral chain materials. Vanadate pyroxenes have been considered owing to their reported high stability and adequate optical properties. We have screened materials with the general formula $[A]VO_3$, with $[A] = NH_4^+$, PH_4^+, H_3O^+, H_3S^+, $CH_3NH_3^+$, $CH(NH_2)_2^+$, and $(C2H5)NH3^+$. We have assessed the potential of this family of compounds with the available experimental information for photovoltaic applications by comparing their carrier transport and optical properties and by focusing onto a one-to-one comparison between $CsVO_3$ and NH_4VO_3. This phase has demonstrated that the hybrid vanadates are as good as their inorganic counterparts in terms of transport properties.

To overcome the obstacle of the large electronic band gap in this family of compounds, we computationally searched for new hybrid vanadates with little or no experimental information. We have shown that full structural relaxation on a sufficiently large supercell is crucial, despite being computationally expensive. Most importantly, we have shown that cation substitution can change the structural properties, sometimes in significant ways. In some cases, this enables one to tune the band gap, as well as the light-absorbing properties, by molecular engineering. We have unveiled two mechanisms to tune the band gap for this class of compounds, namely by inducing crystal field splitting through deformation of the VO_4 tetrahedral network and by molecular deprotonation and the formation of strong hydrogen bonds with the molecular cation. Although the two mechanisms are correlated, the latter yields a more sizable reduction in the band gap with beneficial implications on the optical absorption properties in the visible

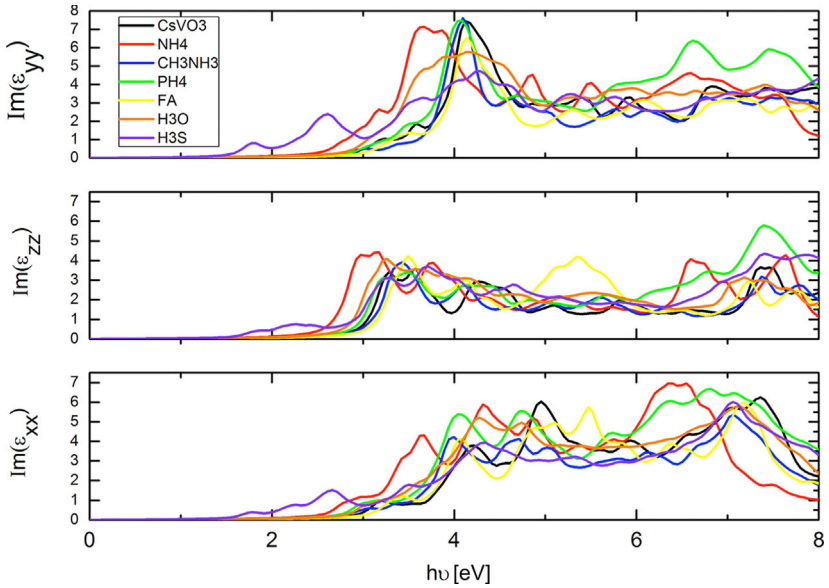

Figure 9. Imaginary part of the frequency-dependent dielectric functions in the independent particle approximations for selected compounds showing molecule-dependent light-absorbing properties.

range of the solar spectrum. We identified H_3SVO_3 as a strong absorber and stable against phase separation and moisture. This compound could attract further experimental investigation and additional computational work is underway.

Acknowledgements

This work was sponsored by the Qatar Environment and Energy Research Institute (F.E., F.H.A., S.R., S.K., G.B., and M.E.M.). Computational resources were provided by the supercomputer facilities at the Trinity Center for High Performance Computing at ICHEC (project tcphy040c) and the research computing at Texas A&M University at Qatar. We are grateful to SHAHEEN supercomputer at King Abdullah University of Science and Technology (KAUST), Saudi Arabia, where the calculations were conducted. This work is supported by the Qatar National Research Fund (QNRF) through the National Priorities Research Program (NPRP8-090-2-047).

Conflict of interest

The authors declare no conflict of interest.

Keywords: density functional calculations · organic–inorganic hybrid composites · photovoltaics · solar cells · vanadium

[1] C. Wadia, A. P. Alivisatos, D. M. Kammen, *Environ. Sci. Technol.* **2009**, *43*, 2072.
[2] F. H. Alharbi, J. D. Bass, A. Salhi, A. Alyamani, H.-C. Kim, R. D. Miller, *Renewable Energy* **2011**, *36*, 2753.
[3] M.-E. Ragoussi, T. Torres, *Chem. Commun.* **2015**, *51*, 3957.
[4] G. R. Timilsina, L. Kurdgelashvili, P. A. Narbel, *Renewable Sustainable Energy Rev.* **2012**, *16*, 449.
[5] V. Devabhaktuni, M. Alam, S. S. S. R. Depuru, R. C. Green, D. Nims, C. Near, *Renewable Sustainable Energy Rev.* **2013**, *19*, 555.
[6] H.-S. Kim, S. H. Im, N.-G. Park, *J. Phys. Chem. C* **2014**, *118*, 5615.
[7] S. D. Stranks, H. J. Snaith, *Nat. Nanotechnol.* **2015**, *10*, 391.
[8] J. Berry, T. Buonassisi, D. A. Egger, G. Hodes, L. Kronik, Y.-L. Loo, I. Lubomirsky, S. R. Marder, Y. Mastai, J. S. Miller, et al., *Adv. Mater.* **2015**, *27*, 5102.
[9] D. P. McMeekin, G. Sadoughi, W. Rehman, G. E. Eperon, M. Saliba, M. T. Hörantner, A. Haghighirad, N. Sakai, L. Korte, B. Rech, M. B. Johnston, L. M. Herz, H. J. Snaith, *Science* **2016**, *351*, 151.
[10] F. H. Alharbi, S. Kais, *Renewable Sustainable Energy Rev.* **2015**, *43*, 1073.
[11] P. Würfel, U. Würfel, *Physics of Solar Cells: From Basic Principles to Advanced Concepts*, 3rd ed., Wiley-VCH, Weinheim, **2016**.
[12] J. Hachmann, R. Olivares-Amaya, S. Atahan-Evrenk, C. Amador-Bedolla, R. S. Sa 'nchez-Carrera, A. GoldParker, L. Vogt, A. M. Brockway, A. Aspuru-Guzik, *J. Phys. Chem. Lett.* **2011**, *2*, 2241.
[13] S. Curtarolo, G. L. Hart, M. B. Nardelli, N. Mingo, S. Sanvito, O. Levy, *Nat. Mater.* **2013**, *12*, 191.
[14] H. P. Lüthi, S. Heinen, G. Schneider, A. Glöss, M. P. Brändle, R. A. King, E. Pyzer-Knapp, F. H. Alharbi, S. Kais, *J. Comput. Sci.* **2016**, *15*, 65.
[15] F. H. Alharbi, S. N. Rashkeev, F. El-Mellouhi, H. P. Lüthi, N. Tabet, S. Kais, *NPJ Comput* **2015**, *1*, 15003.
[16] G. Volonakis, M. R. Filip, A. A. Haghighirad, N. Sakai, B. Wenger, H. J. Snaith, F. Giustino, *J. Phys. Chem. Lett.* **2016**, *7*, 1254.
[17] T. Hiortdahl, *Z. Kristallogr.-Crystal. Mater.* **1882**, *6*, 456.
[18] D. B. Mitzi, C. Feild, Z. Schlesinger, R. Laibowitz, *J. Solid State Chem.* **1995**, *114*, 159.
[19] K. Chondroudis, D. B. Mitzi, *Chem. Mater.* **1999**, *11*, 3028.
[20] C. R. Kagan, D. Mitzi, C. Dimitrakopoulos, *Science* **1999**, *286*, 945.
[21] B. Mitzi, C. D. Dimitrakopoulos, L. L. Kosbar, *Chem. Mater.* **2001**, *13*, 3728.
[22] D. B. Mitzi, *J. Chem. Soc. Dalton Trans.* **2001**, 1 – 12.
[23] J. S. Manser, J. A. Christians, P. V. Kamat, *Chem. Rev.* **2016**, *116*, 12956.
[24] D. B. Mitzi, K. Chondroudis, C. R. Kagan, *IBM J. Res. Dev.* **2010**, *45*, 29.
[25] S. N. Rashkeev, F. El-Mellouhi, S. Kais, F. H. Alharbi, *Sci. Rep.* **2015**, *5*, 11467.
[26] G. R. Berdiyorov, F. El-Mellouhi, M. E. Madjet, F. H. Alharbi, S. N. Rashkeev, *Appl. Phys. Lett.* **2016**, *108*, 053901.
[27] C. Motta, F. El-Mellouhi, S. Sanvito, *Sci. Rep.* **2015**, *5*, 12746.
[28] C. Persson, A. Zunger, *Phys. Rev. Let.* **2003**, *91*, 266401.
[29] L. G. Tejuca, J. Fierro, *Properties and Applications of Perovskite-Type Oxides* CRC Press, Boca Raton, FL **2000**.
[30] H. S. C. O'Neill, A. Navrotsky, *Am. Mineral.* **1983**, *68*, 181.
[31] D. Adams, A. Christy, J. Haines, *J. Phys. Condens. Matter* **1991**, *3*, 6135.
[32] F. Hawthorne, C. Calvo, *J. Solid State Chem.* **1977**, *22*, 157.
[33] M. Weckhuysen, D. E. Keller, *Catal. Today* **2003**, *78*, 25.
[34] C. Costa, C. Pinheiro, I. Henriques, C. A. T. Laia, *ACS Appl. Mater. Interfaces* **2012**, *4*, 5266.
[35] M. Najdoski, V. Koleva, A. Samet, *Dalton Trans.* **2014**, *43*, 12536.
[36] N. Bahlawane, D. Lenoble, *Chem. Vap. Deposition* **2014**, *20*, 299.
[37] T. Nakajima, M. Isobe, T. Tsuchiya, Y. Ueda, T. Kumagai, *J. Lumin.* **2009**, *129*, 1598.
[38] T. Nakajima, M. Isobe, Y. Uzawa, T. Tsuchiya, *J. Mater. Chem. C* **2015**, *3*, 10748.
[39] Q. Chen, N. De Marco, Y. M. Yang, T.-B. Song, C.-C. Chen, H. Zhao, Z. Hong, H. Zhou, Y. Yang, *Nano Today* **2015**, *10*, 355.
[40] F. El-Mellouhi, E. T. Bentria, S. N. Rashkeev, S. Kais, F. H. Alharbi, *Sci. Rep.* **2016**, *6*, 30305.
[41] F. El-Mellouhi, E. T. Bentria, A. Marzouk, S. N. Rashkeev, S. Kais, F. H. Alharbi, *NPJ Comput.* **2016**, *2*, 16035.
[42] F. El-Mellouhi, A. Marzouk, E. T. Bentria, S. N. Rashkeev, S. Kais, F. H. Alharbi, *ChemSusChem* **2016**, *9*, 2648.
[43] V. Blum, R. Gehrke, F. Hanke, P. Havu, V. Havu, X. Ren, K. Reuter, M. Scheffler, *Comput. Phys. Commun.* **2009**, *180*, 2175.
[44] A. Tkatchenko, M. Scheffler, *Phys. Rev. Lett.* **2009**, *102*, 073005.
[45] C. Motta, F. El-Mellouhi, S. Kais, N. Tabet, F. Alharbi, S. Sanvito, *Nat. Commun.* **2015**, *6*, 7026.
[46] J. Monkhorst, J. D. Pack, *Phys. Rev. B* **1976**, *13*, 5188.
[47] H. Press, S. A. Teukolsky, W. T. Vetterling, B. P. Flannery, *Numerical Recipes in C*, 2nd ed., Cambridge University Press, Cambridge, **1996**.
[48] B. Wang, J. Wang, H. Guo, *Phys. Rev. Lett.* **1999**, *82*, 398.
[49] G. Kresse, J. Furthmüller, *Comput. Mater. Sci.* **1996**, *6*, 15.
[50] G. Madsen, D. Singh, *Comput. Phys. Commun.* **2006**, *175*, 6771.
[51] Y. Wang, J. Lv, L. Zhu, Y. Ma, *Comput. Phys. Commun.* **2012**, *183*, 2063.
[52] M. Hellenbrandt, *Crystallogr. Rev.* **2004**, *10*, 17.
[53] T. Nakajima, M. Isobe, T. Tsuchiya, Y. Ueda, T. Manabe, *J. Phys. Chem. C* **2010**, *114*, 5160.
[54] J. Heyd, G. E. Scuseria, M. Ernzerhof, *J. Chem. Phys.* **2003**, *118*, 8207.
[55] S. Hayakawa, T. Yoko, S. Sakka, *Bull. Chem. Soc. Jpn.* **1993**, *66*, 3393.
[56] M.-T. Averbuch-Pouchot, A. Durif, *C. R. Acad. Sci. Ser. II* **1994**, *319*, 1013.
[57] L. Smrčok, B. Bitschnau, Y. Filinchuk, *Cryst. Res. Technol.* **2009**, *44*, 978.
[58] N. Wadnerkar, N. J. English, *Comput. Mater. Sci.* **2013**, *74*, 33.
[59] C. Motta, F. El-Mellouhi, S. Sanvito, *Phys. Rev. B* **2016**, *93*, 235412.
[60] M. E. Madjet, A. V. Akimov, F. El-Mellouhi, G. R. Berdiyorov, S. Ashhab, N. Tabet, S. Kais, *Phys. Chem. Chem. Phys.* **2016**, *18*, 5219.
[61] P. Azarhoosh, J. M. Frost, S. McKechnie, A. Walsh, M. van Schilfgaarde, arXiv:1604.04500, **2016**.
[62] W. Setyawan, S. Curtarolo, *Comput. Mater. Sci.* **2010**, *49*, 299.
[63] F. El-Mellouhi, E. N. Brothers, M. J. Lucero, I. W. Bulik, G. E. Scuseria, *Phys. Rev. B* **2013**, *87*, 035107.
[64] F. El-Mellouhi, E. N. Brothers, M. J. Lucero, G. E. Scuseria, *Phys. Rev. B* **2011**, *84*, 115122.
[65] V. Peet, *J. Opt.* **2010**, *12*, 095706.
[66] D. Banabic, F. Barlat, O. Cazacu, T. Kuwabara, *Int. J. Mater. Forming* **2010**, *3*, 165.
[67] P. Weightman, D. Martin, R. Cole, T. Farrell, *Rep. Prog. Phys.* **2005**, *68*, 1251.
[68] A. H. Nayfeh, *Wave Propagation in Layered Anisotropic Media: with Application to Composites*, Elsevier, Amsterdam, **1995**.

[69] G. R. Berdiyorov, A. Kachmar, F. El-Mellouhi, M. A. Carignano, M. E. Madjet, *J. Phys. Chem. C* **2016**, *120*, 16259.
[70] A. Binek, F. C. Hanusch, P. Docampo, T. Bein, *J. Phys. Chem. Lett.* **2015**, *6*, 1249.
[71] M. R. Dolgos, A. M. Paraskos, M. W. Stoltzfus, S. C. Yarnell, P. M. Woodward, *J. Solid State Chem.* **2009**, *182*, 1964.
[72] E. Arunan, G. R. Desiraju, R. A. Klein, J. Sadlej, S. Scheiner, I. Alkorta, D. C. Clary, R. H. Crabtree, J. J. Dannenberg, P. Hobza, et al., *Pure Appl. Chem.* **2011**, *83*, 1637.
[73] J.-C. Hebig, I. Kühn, J. Flohre, T. Kirchartz, *ACS Energy Lett.* **2016**, *1*, 309.
[74] Z. Deng, F. Wei, S. Sun, G. Kieslich, A. K. Cheetham, P. D. Bristowe, *J. Mater. Chem. A* **2016**, *4*, 12025.
[75] M. A. Carignano, Y. Saeed, S. A. Aravindh, I. S. Roqan, J. Even, C. Katan, *Phys. Chem. Chem. Phys.* **2016**, *18*, 27109.
[76] M. Saliba, T. Matsui, J.-Y. Seo, K. Domanski, J.-P. Correa-Baena, M. K. Nazeeruddin, S. M. Zakeeruddin, W. Tress, A. Abate, A. Hagfeldt, M. Grätzel, *Energy Environ. Sci.* **2016**, *9*, 1989.

Manuscript received: January 22, 2017
Accepted Article published: February 5, 2017
Final Article published: ■■ ▮▮, 0000

A chain for the better: A new class of materials for photovoltaic applications has been developed, based on low-dimensional hybrid vanadate pyroxenes $[A]VO_3$ (with molecular cations [A] and corner-sharing VO_4 tetrahedral chains). These materials were found to satisfy the physical requirements needed to develop an efficient solar cell (a band gap of 1.0–1.7 eV, strong light absorption and good electron-transport properties).

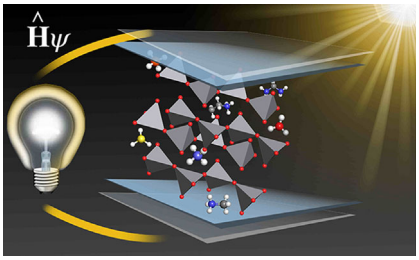

F. El-Mellouhi, A. Akande,* C. Motta, S. N. Rashkeev, G. Berdiyorov, M. E. Madjet, A. Marzouk, E. T. Bentria, S. Sanvito, S. Kais, F. H. Alharbi**

■■ – ■■

Solar Cell Materials by Design: Hybrid Pyroxene Corner-Sharing VO_4 Tetrahedral Chains